Silver nanoparticles self assembly as SERS substrates with near single molecule detection limit

Meikun Fan and Alexandre G. Brolo*

Received 9th March 2009, Accepted 4th June 2009
First published as an Advance Article on the web 15th July 2009
DOI: 10.1039/b904744a

Highly sensitive SERS substrates with a limit of detection in the zeptomole (for Nile blue A and oxazine 720) range were fabricated through a bottom-up strategy. Ag nanoparticles (Ag NPs) were self-assembled onto glass slides by using 3-mercaptopropyltrimethoxysilane (MPTMS) sol–gel as linker. The substrates were characterized by UV-Vis and AFM after each deposition of Ag NPs. It was found that the glass slide presented just a few Ag NPs aggregates scattered throughout the surface after just one deposition. The glass surface was gradually covered by a homogeneous distribution of Ag NPs aggregates as the deposition number increased. Surface-enhanced Raman scattering (SERS) of the substrates was examined at different numbers of Ag NPs deposition using nile blue A and oxazine 720 as probe molecules and two laser excitations (632.8 nm and 785 nm). Optimum SERS was observed after six depositions of Ag NPs. SERS mapping indicated that at lower deposition numbers (less than 3 Ag NPs depositions) the substrates presented a few SERS ''hot–spots'' randomly distributed at the surface. After 7 Ag NPs depositions, spatial distribution of the SERS signal followed a Gaussian statistics, with a percent relative standard deviation (RSD%) of $\sim$19%. In addition, the sample-to-sample reproducibility of the SERS intensities under both laser excitations was lower than 20%. It was also found that these substrates can provide giant Raman signal enhancement. At optimum conditions and with a 632.8 nm laser, the signal from an estimated of only $\sim$44 probe molecules (100$\times$ objective) can still be detected.

I. Introduction

After more than 30 years of development, surface-enhanced Raman scattering (SERS)[1–4] has been proved as a versatile analytical technique.[5] This is not only due to its high sensitivity but also because SERS provides vibrational (fingerprint) information of target molecules. The analytical capabilities of SERS have been explored in several fields, including environmental sciences and biomedicine.[6–10] For example, SERS has been used to detect DNA,[11] enzymes,[7] and even to follow enzymatic activity in a single cell.[6] In addition, SERS-based immunoassays are widely reported and provide several advantages relative to other labeling techniques, in terms of sensitivity, selectivity and multiplexing.[9,10] SERS detection has also been used in environmental analysis for the detection of polycyclic aromatic hydrocarbons in aqueous solution.[12,13]

The enhancement of local electromagnetic fields *via* localized surface plasmon modes in metallic nanostructures is mostly responsible for the SERS phenomena.[5,14–16] This field localization is controlled by the nanostructure morphology. Hence, there are tremendous efforts to explore different nanostructures that support SERS, aiming at optimized substrates with high sensitivity and reproducibility.

SERS substrates can be prepared using either the bottom-up or the top-down strategy. The electrochemical roughening of electrodes through oxidation–reduction cycles (ORCs) is among the simplest example of a SERS substrate.[1,17] However, this technique does not allow much control over the size and shape of the nanofeatures, leading to low reproducibility. Recently, more elaborated top-down strategies have become accessible due to the latest developments in nanolithography. Modern nanofabrication methods allow tailoring of the nanostructures for maximum enhancement, and the fabrication of reproducible nanofeatures even in a large area.[18–20] For example, periodic arrays of sub-wavelength apertures (nanoholes) have been proved to be successful SERS substrates.[21–24] SERS from single nanoholes has also been observed.[25] Other top-down fabricated nanostructures for SERS reported recently include: Au nanoparticle arrays;[26,27] ''multi-bowtie''[28] structures; Au nano-disks with different thickness and separation distances;[29] and gold moon crescent structures.[30] Some of these structures have been proved to have a close to single-molecule detection limit.[25,28,30] However, the common disadvantage among some of these top-down methodologies is their high cost per fabricated sample and their serial character (such as in focused-ion beam milling and in electron beam lithography). A cheaper alternative is the preparation of SERS substrates by the self-assembly of metallic nanoparticles (bottom-up approach). The building blocks in this case are nanoparticles (NPs) of different shapes (nanospheres, nanorods, nanocubes) and compositions, including core-shell structures.[31] The NPs are immobilized in a planar platform through either covalent[32–36] or

Department of Chemistry, University of Victoria, Victoria, Canada, BC V8W 3V6. E-mail: agbrolo@uvic.ca

non-covalent[37–43] interactions with linkers. The "linkers" generally used for non-covalent self-assembly are organic polymers[44] and polymer dendrimers,[38,45] DNAs,[37] and proteins;[42,43] as for covalent self-assembly, organic silane[32] and dithiols[33–35] are common choices. The preparation of positively charged Ag NPs[46] and their application in the multi-layer self-assembly of oppositely charged NPs as SERS substrates[47,48] has also been reported. The bottom-up approach, however, commonly provides less spatial and sample-to-sample reproducibility than the nanolithographic methods.

Previously, we have reported a bottom-up strategy to fabricate SERS substrates using Au NPs.[33,34] 1,3-Propanedithiol was used as a linker for the multiple depositions of Au NPs onto both glass and gold slides. It was found that the SERS signal maximizes after a certain number of Au NPs depositions at a given excitation energy. Meanwhile, the spatial variation of the SERS signal and the optimized sample to sample reproducibility obtained by this procedure were lower than 20%.[34]

In this report, we will present a self-assembled substrate for SERS based on Ag NPs as building blocks and 3-mercaptopropyltrimethoxysilane (MPTMS) sol–gel as linker. Although dithiols proved to be good linkers for the stepwise deposition of Au NPs,[33–35] they are not as efficient for Ag NPs deposition. Alternative approaches for Ag immobilization include thiol-exchange reactions[49] and layer-by-layer deposition through electrostatic interactions.[37,38,40,47,48] The limited success of the application of dithiol as a linker to the fabrication of self-assembled Ag structures is probably due to the strong affinity of the thiol functionality towards the Ag surface which favors the simultaneous interaction of both thiol groups of the dithiol with the Ag, leaving no free thiol group to interact with the adjacent layer.[50] Hydrolyzation of MPTMS leads to the formation of a sol–gel rich in free thiol functionalities,[51] which guarantees the availability of thiol groups after binding to the bottom layer of Ag NPs. It was found in this report that the SERS efficiency increases with the number of Ag NPs deposition, stabilizing after 6 depositions for both 632.8 nm and 785 nm laser excitations. These results agree with our previous work involving Au NPs deposition on Au films.[34] The spatial variation of the SERS signal also decreased with increasing Ag NPs depositions, as revealed by SERS mapping. In addition, slide-to-slide variations in SERS intensities proved to be less than 20% for both lasers used. Finally, this class of substrates is very sensitive, allowing the detection of about 44 Nile blue A (NBA) molecules at 632.8 nm excitation using a 100× objective.

II. Experimental

2.1 Chemicals

Unless otherwise mentioned, ACS grade chemicals were used. $AgNO_3$, sodium citrate dihydrate, 3-mercaptopropyltrimethoxysilane (MPTMS), Oxazine 720 and Nile blue A (NBA) perchlorate were obtained from Sigma-Aldrich. Ultrapure water with a resistivity of 18.2 MΩ cm (from Barnstead NANOpure Diamond water purification system) was used throughout the experiments. Glass slides are 1 × 1 inch regular microscope slides.

2.2 Synthesis of Ag NPs and MPTMS sol–gel

The preparation of Ag NPs followed the procedure reported in the literature.[52] Briefly, a 500 mL $AgNO_3$ solution (1 mM) was heated to ~90 °C (initial boiling) under vigorous stirring. Then, 20 mL of 1% sodium citrate solution was quickly added. The solution was kept on a hotplate with stirring until it turned into an apparent luminescent yellow. After that, the hotplate was removed but stirring was kept until the solution cooled down to room temperature (about 25 °C). The as prepared Ag NPs showed an absorption peak at 407 nm.

The MPTMS sol–gel preparation also follows the literature[51] but with some modifications. Briefly, 600 μL of MPTMS and 500 μL of 0.1 M HCl were added into 50 mL of water. The solution was vigorously stirred for at least 1 h. The sol–gel solution should be used the same day.

2.3 Preparation of the SERS substrate

The glass slides were cleaned using piranha solution and rinsed thoroughly with water. Then, they were dried using a nitrogen flow, rinsed with methanol and soaked in 10 mM MPTMS methanolic solution for 24 h. The modified slides were then rinsed with copious amounts of methanol, dried with nitrogen, rinsed again with water, and finally immersed into the Ag NPs solution for another 24 h. For the deposition of additional Ag NPs, the slides were removed from the Ag NPs solution, thoroughly rinsed with water and dipped into the MPTMS sol–gel for 20 min and then immersed again in the Ag NPs solution for 1 h. This procedure was repeated until the desired number of Ag NPs depositions was achieved. Rigorous rinsing was performed after each step.

2.4 Characterization of the SERS substrate

The UV-Vis spectra of the slides were obtained using a UV-visible spectrometer (Agilent, model 8453). The spectrum of a clean glass in air was used as background. AFM scans were accomplished using a Nanonics Imaging AFM model MV-1000. Intermittent contact mode was used with a pulled glass fiber tip. The image was analyzed with WSXM software.

2.5 SERS measurement

All the Raman measurements were accomplished using a RENISHAW inVia Raman microscope system equipped with a He–Ne and a diode near IR as laser sources. The He-Ne excitation, at 632.8 nm (6.7 μW), presented a circular laser spot at the sample with a diameter (FWHM) equal to 0.9 μm for the 50× objective and equal to 0.5 μm for the 100× objective. The laser spot of the diode near IR laser, at 785 nm (0.317 mW), was a rectangle of 2.6 μm × 5.8 μm for the 50× objective.

The SERS probes (Nile blue A and oxazine 720) were added to the substrates as follows: An appropriate amount of the dyes were dissolved in methanol. Then, 50 μL of the solution was dropped onto the 1 × 1 inch substrate. This amount of

solution covered the whole surface. The slides were then left in air to dry.

To calculate the amount of probe molecules in the laser spot region, the number of moles of the probe molecule was calculated from the solution concentration and then divided by the surface area of the glass slide, yielding moles per unit area, which was then multiplied by the size of the laser spot. Note that this calculation is based on the assumption that the binding constant of the probe molecules to the substrate is infinitely high. Thus, the estimated number N of adsorbed molecules is an upper limit.

III. Results and discussion

3.1 Substrate characterization

Scheme 1 represents the procedure used in the preparation of the SERS substrates used in this work. A clean glass slide was initially modified with MPTMS. The modified slide was dipped into an Ag NPs solution for 24 h. The Ag NPs interact with the pendant thiol groups of the MPTMS, forming the first layer of NPs. Further addition of NPs was accomplished by dipping the slide with the first layer of Ag NPs in MPTMS sol–gel for 20 min. The MPTMS sol–gel "polymer" attach to the Ag NPs but leaves free thiols for the deposition of the next Ag NPs layer. The last two steps were repeated until the desired number of Ag NPs depositions was achieved.

A common disadvantage of linker-based SERS substrates is the Raman signature of the linker molecules (the sol–gel "polymer", in our case), which will be a constant background

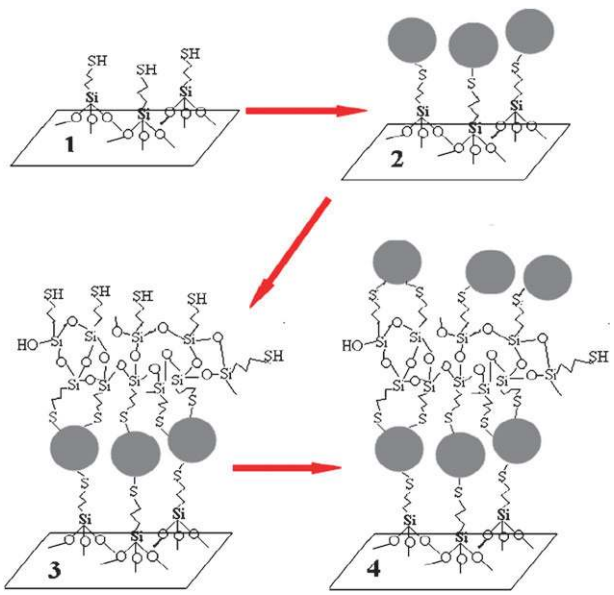

Scheme 1 Preparation of the SERS substrates. This diagram is not to scale. Step 1: The surface of a clean glass slide is modified by MPTMS to yield pedant thiol groups; Step 2: The modified glass slide is immersed in a solution of Ag NPs (grey circles), which will adhere to the surface by interacting with the thiol groups; Step 3: The slide is dipped in a sol–gel of MPTMS to add more thiol functionalities to the surface; Step 4: The substrate is immersed again in a solution of Ag NPs to receive an additional layer of Ag NPs. Steps 3 and 4 are repeated until the desired number of depositions is achieved.

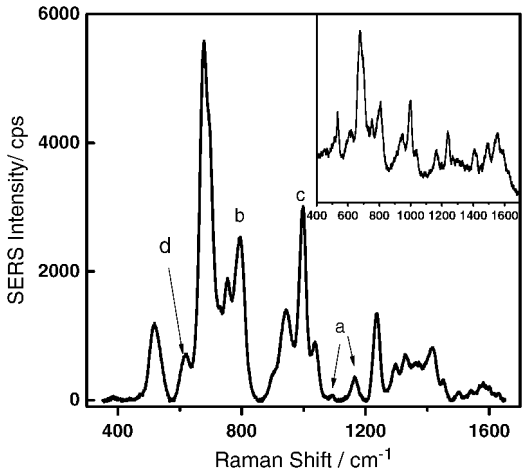

Fig. 1 SERS spectrum from Ag NPs substrate after 7 Ag NPs depositions. There are no probe molecules adsorbed at the silver surface and the spectrum corresponds to the background due to the sol–gel polymer. Laser excitation at 785 nm. The inset shows the spectrum of the same sample obtained using 632.8 nm excitation.

in the SERS experiments. Fig. 1 shows the spectra of the SERS substrate after the deposition of 7 Ag NPs "layers" for both laser excitations used in this work. The Raman signature in Fig. 1 is typical for hydrolyzed MPTMS. For instance, the bands labeled as *a* have been assigned to the longitudinal and transverse optical (LO and TO) stretching modes of Si–O–Si, and the *b* band is the symmetrical stretch of the Si–O–Si network.[53,54] The peaks labeled *c* and *d* are from SiOH modes, implying some defects in the polymeric network.[53,55] The background spectrum presented in Fig. 1 will not be a significant spectral interference for SERS of strong scattering. However, the background does become important during the detection of a small number of adsorbates, as will be discussed later.

The morphologies of the SERS substrates prepared in this work were monitored by AFM, and a few representative images are presented in Fig. 2. It is clear from the AFM that the packing density and the homogeneity of the surface features increased with the number of Ag NPs deposition. The height of the features in Fig. 2a was between 40–90 nm, which is in agreement with the particle size distribution of the synthesized Ag colloid.[52] All AFM images presented features with average lateral dimensions between 200–400 nm, except for Fig. 2a (1 Ag NP deposition) that shows a few clusters with lateral dimensions of less than 100 nm.

Fig. 3 shows the UV-Vis absorption of the substrates prepared with different numbers of Ag NPs depositions. A typical surface plasmon absorption band was observed at 409 nm for the substrate with just one deposition of Ag NPs. This absorption maximum red-shifted with the increasing number of Ag NPs deposition, quickly reaching 446 nm after 7 depositions of Ag NPs, and shifting only slightly after that. An absorption shoulder at around 680 nm appears after 3 depositions of Ag NPs, and the absorption band tails towards the near IR (*ca.* 1000 nm) region as the number of Ag NPs deposition increases. These results are common indications of Ag NPs aggregation, which become more significant with the

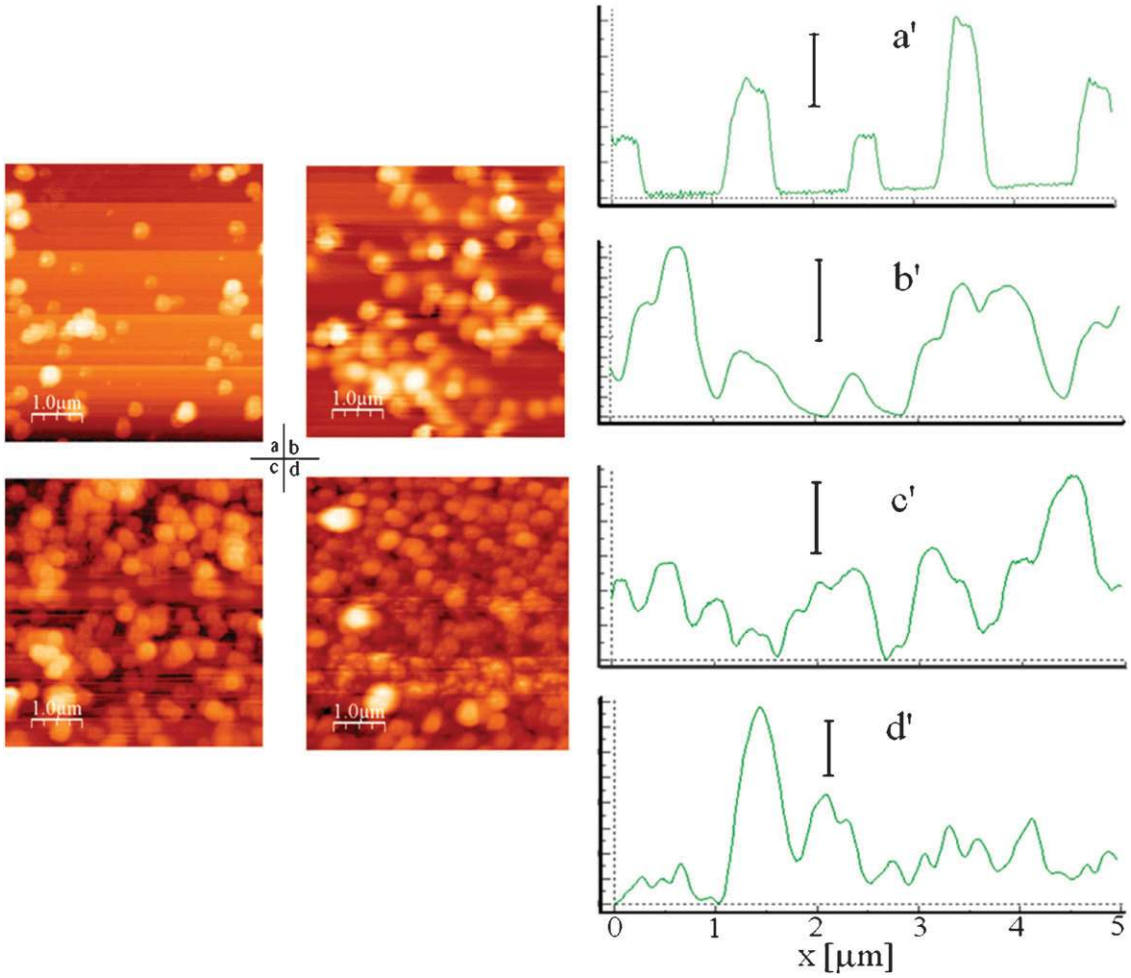

Fig. 2 AFM images of the Ag NPs substrates after (a) 1; (b) 3; (c) 5; and (d) 7 depositions of Ag NPs. The representative line profiles of the images are shown in a′, b′, c′ and d′, respectively. Scale bar shows 40 nm.

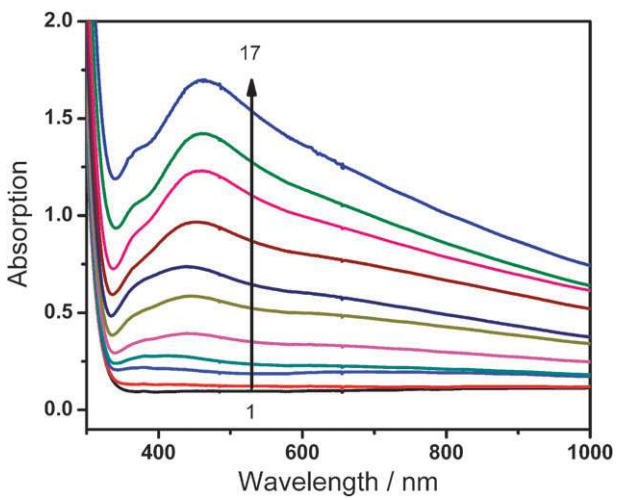

Fig. 3 UV-Vis absorption of Ag NPs modified slides. From bottom to top: 1, 2, 3, 4, 5, 7, 9, 11, 13, 15, 17 deposition(s) of Ag NPs on glass.

increase in the amount of Ag NPs.[44] The optical data agrees with the increase in nanoparticle density with the number of Ag NPs depositions shown in the AFM images in Fig. 2.

3.2 SERS performance

3.2.1 Substrate optimization for SERS. Nile blue A (NBA) and oxazine 720 were used as molecular probes to evaluate the SERS performance of the Ag NPs modified slides. Both dyes have a very similar structure and have electronic absorptions in the region of the 632.8 nm excitation. Therefore, experiments using that excitation wavelength contain contributions from the resonance Raman effect (surface-enhanced resonance Raman scattering (SERRS)). The dependence of the SER(R)S intensity of the *ca.* 593 cm^{-1}-band of NBA with the number of Ag NPs depositions is presented in Fig. 4. Experiments were carried out for two laser excitations: 632.8 nm and 785 nm. The SER(R)S intensities in Fig. 4 are averages of 5 measurements from different spots of the slide surface and the error bars represent the standard error of these measurements. The SERS spectrum in the inset for 785 nm excitation presents a weak broad shoulder around 680 cm^{-1} (indicated with an arrow), but this feature is absent in the case of 632.8 nm excitation. This shoulder is a background contribution from the substrate (Fig. 1). Notice that no resonance Raman contribution is expected at 785 nm, but an additional Raman resonance effect is present at 632.8 nm excitation (SERRS effect) and the background signal from the substrate is

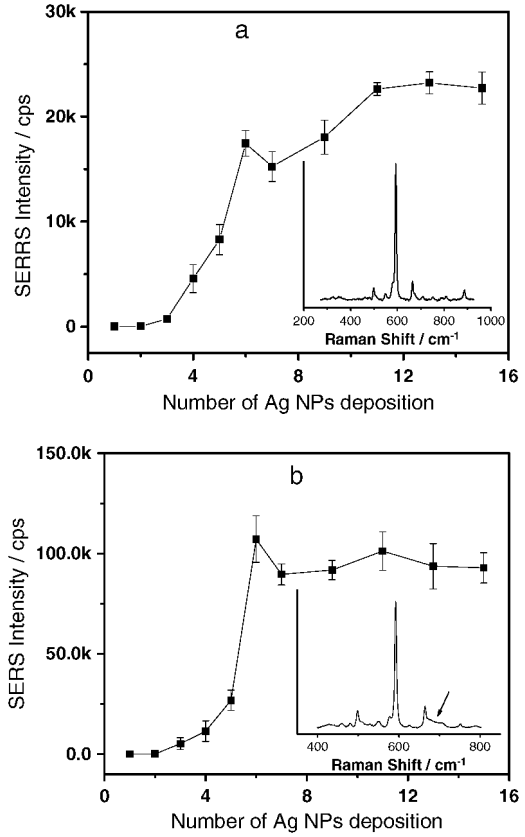

Fig. 4 SERS performance of the Ag NPs-modified glass slides. NBA was used as the molecular probe and its 593 cm^{-1}-band is plotted against the number of Ag NPs depositions. (a) 632.8 nm excitation and power density equal to 10 $\mu W/\mu m^2$; (b) 785 nm excitation and power density equal to 21 $\mu W/\mu m^2$. The amount of NBA on each slide was constant (4 μg/ml). 5 measurements were performed in different regions of each sample and the SER(R)S results were averaged. The bars show the standard error (SE) that represents this spatial variation. Insets show SER(R)S spectrum of NBA on a substrate after 7 Ag NPs deposition for each excitation.

negligible in that condition. The higher intensity (in cps) observed for the 785 nm excitation (Fig. 4b) is due to the larger power density and illuminated area for this excitation.

After 6 Ag NP depositions, the SER(R)S signal reached a maximum and stabilized after the peak, although some increase is still noted in Fig. 4a. It is difficult to rationalize the reason for this stabilization without any knowledge of the evolution of the near field distribution within the different morphologies, although an increase in scattering loss from large nanofeatures should contribute to this effect. The behavior, however, is in agreement with our previous results from Au NPs deposited on gold slides.[34] Interestingly, we didn't observe the strong dependence on the optimum SERS with the excitation wavelength as observed for Au NPs deposited in glass using a dithiol linker.[33] This may be rationalized by considering the differences in particle size and morphology between these substrates (Au deposited on glass using dithiol linkers[33] and Ag deposited on glass using MPTMS sol–gel (this work)). As shown in Fig. 2a to d, the coverage of Ag NPs aggregates changed with increasing deposition. This can be further confirmed from the line profiles in Fig. 2b′ to d′, which show almost no change in the lateral dimensions of the nanostructures with increasing deposition numbers. This behavior differs from the results observed using Au NPs, where lateral sizes of the features increased with increasing deposition number.[33] This is a fundamental difference, certainly related to the nature of the linker, which might explain the different trends in SERS intensities observed from both Ag and Au deposited on glass.

The SER(R)S intensity obtained after 6 Ag NP depositions, normalized by the excitation conditions, from just one Ag NP deposition was about 2 orders of magnitude higher than what was observed for Au NPs.[33,34] Fig. 4 also shows that the SERS signal increased as a power function up to the peak at 6 depositions of Ag NPs, where our former result on Au showed roughly a linear increase until the maximum.[34] Zhu *et al.*[56] considered that SERS intensities should depend on both size and population (*i.e.* inter-particle distance) of NPs, and they showed that there is a threshold particle density where the interaction between the particles become significant. When the population is lower than this threshold, the SERS intensity increased slowly with the particle density. However, the SERS intensity will increase rapidly due to the surface plasmons (SPs) coupling after the threshold value is reached. This effect is especially prominent for NPs with larger size, which is the case here.

The insets in Fig. 5 are the SERRS mappings from the Ag NPs substrate surfaces obtained using the 632.8 nm laser. The spatial distribution of SERRS intensity (in terms of peak area, see the caption in Fig. 5) can also be visualized in Fig. 5 by the analysis of the histograms obtained from these maps. The statistics of the mappings were performed using a method proposed by Scott.[57] The histogram shows the distribution of SERRS intensities (normalized by the average). The inset in Fig. 5a shows that, for 1 Ag NPs deposition, there are several regions at the surface with weak SERS activity. This is confirmed by the large number of events with "zero" intensity in the histogram. In this case, more than one third of the surface area of the substrate presents very low SERRS intensity, although regions with SERRS signals as high as 32 times the average were also observed, indicating the presence of a SERS hot-spot.[3,16] A skewed spatial distribution of SERRS intensities is also observed after 3 and 5 depositions, respectively (Fig. 5b and c). After 3 Ag NPs depositions (Fig. 5b), the distribution of the SERRS signal narrows, and the distribution peak maximum appear closer to 1 (average) compared with that of Fig. 5a. The same observation was recorded after 5 Ag NPs depositions (Fig. 5c). A dramatic change in the shape of the distribution is observed after 7 Ag NPs depositions (Fig. 5d). The distribution in this case presents a normal (Gaussian) profile, with the distribution maximum centered at 1. Also note that the long distribution tails seen in Fig. 5a, 5b and 5c are not evident any more after 7 Ag NPs depositions (Fig. 5d). The spatial variability of SERS intensity calculated from the FWHM of the Gaussian distribution from Fig. 5d is about ±20%. The mapping results from Fig. 5 indicate that the spatial variation of the SERRS intensities were greatly improved after 7 Ag NPs depositions.

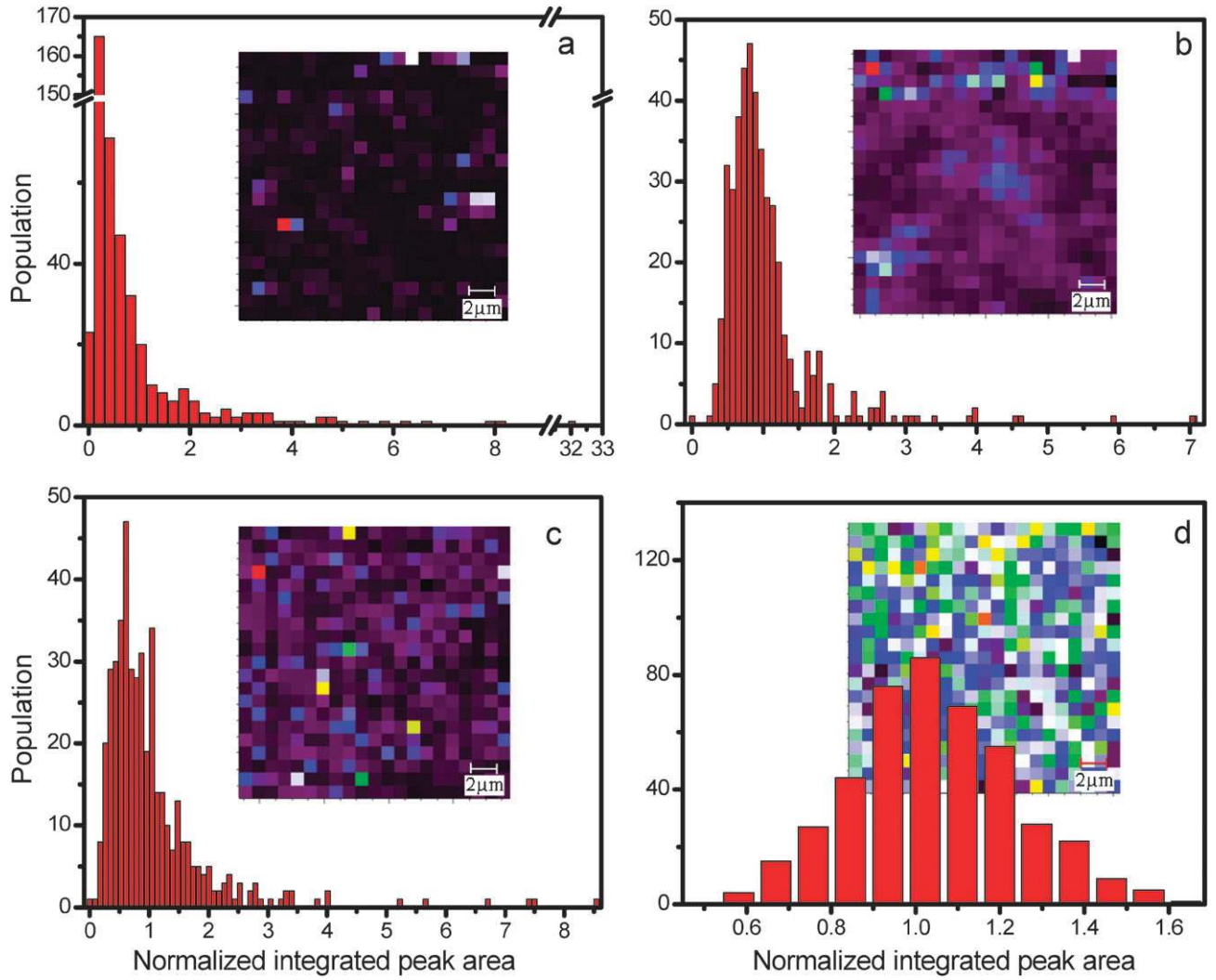

Fig. 5 SERRS mapping of the substrates coated with oxazine 720. Laser excitation at 632.8 nm. The diagrams plot the area of the dominant oxazine 720 SERRS peak at around 595 cm^{-1}. *a* to *d* represents the SERRS intensity (in peak area) distributions from the respective SERRS maps (inset). Note that the intensities for the histograms were normalized using the average SERRS intensity (in peak area).

3.2.2 Sample-to-sample reproducibility of SERS measurements. The sample-to-sample reproducibility of the slides prepared using our self-assembly procedure was tested and the results are presented in Fig. 6. Three different slides were used and the experiments were carried out at both excitations (632.8 nm and 785 nm). The SER(R)S intensity from each slide is the average from 10 randomly chosen spots and the error bars in Fig. 6 represent the calculated standard error (SE) for the spatial variation of the SER(R)S signal. The RSD% (among different slides) on the mean SERRS intensities is less than 10% for 632.8 nm excitation, but the RSD% under 785 nm is 18%. The difference in the spatial variation of SERS intensity for the same molecule at the same substrate but at different excitation wavelengths is an interesting effect. We attribute this difference to the nature of SP modes excited within the illuminated area at the laser frequency. It is anticipated that different SP-modes (surface features) are responsible for SERS at different wavelengths. The spatial distribution of surface structures that provide optimum SERS (hot spots) at 632.8 nm and 785 nm are not expected to be the same. This interesting result highlights the fact that a SERS substrate is "optimized" (not only in terms of enhancement efficiency but also in terms of reproducibility) for a particular excitation wavelength.

3.3 Limit of detection (LOD) for the probe molecule NBA

The quality of the SERS substrate may also be evaluated by its limit of detection (LOD) for a particular molecular probe. Fig. 7 shows the spatially-averaged SERRS spectra of NBA obtained at different concentrations. A fluorescence-like background, present in some spectra, was corrected, and the spectra at lower concentrations were multiplied by a constant for better comparison. The strong bands at $\sim$509 cm^{-1}, $\sim$677 cm^{-1}, $\sim$750 cm^{-1} are from the substrate (Fig. 1), but the NBA band (marked with an asterisk (*) in Fig. 7) can still be clearly identified at very low analyte concentrations (Fig. 7a). Even the dominant band from the substrate at $\sim$677 cm^{-1} doesn't constitute a strong interference at higher concentrations of the dye for 633 nm excitation (100 ng/mL,

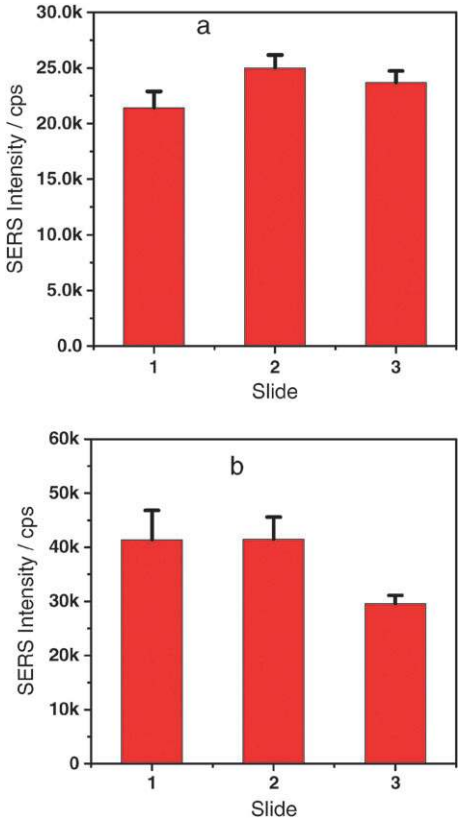

Fig. 6 Spatially-averaged SER(R)S intensities (at 593 cm^{-1}) for three 7-Ag NPs-deposition slides. (a) 632.8 nm; (b) 785 nm. The error bar shows the standard error of the spatial distribution of SER(R)S intensity. Concentration of NBA: 4 μg/ml.

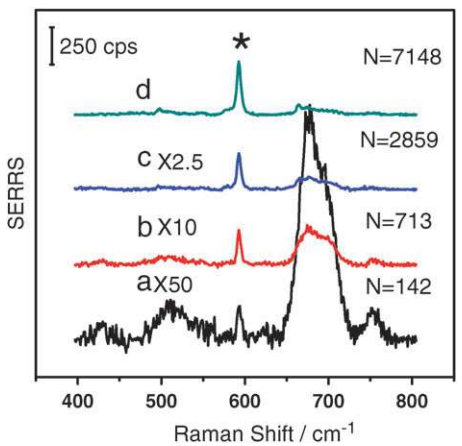

Fig. 7 Spatially-averaged (5 measurements) SERRS spectra at different concentrations of NBA (background corrected). (a) 2 ng/mL; (b) 10 ng/mL; (c) 40 ng/mL; (d) 100 ng/mL. Spectra *a* to *c* were multiplied by a constant shown in the figure. Laser excitation was 632.8 nm and the substrate with 7 Ag NPs depositions were used. *N* is the estimated number of molecules within the laser spot. The asterisk (*) marks the position of the strongest NBA band.

Fig. 7d), showing the strong efficiency of the SERRS effect in this case. The number of molecules in the laser spot, N, was calculated assuming a uniform coverage of the whole surface (see experimental section for details). SERRS was still observed even when only 142 molecules were estimated to populate the laser spot at 632.8 nm excitation and a 50× objective lens. Since it is unlikely that all 142 molecules populate hot-spots inside the laser illuminated region, it is possible that the amount of molecules that are actually contributing to the observed signal is even smaller.

This is better illustrated in Fig. 8, where a SERRS mapping was performed for a sample with only ~142 molecules estimated in the laser spot. Since the coverage of NBA is small (assuming NBA molecule lies flat on the substrate (the maximum space it can occupy), the coverage would be roughly 0.06%), the chance of NBA molecules finding a hot spot is also small. Furthermore, the distribution of hot spots and the distribution of molecules are two independent factors, and the combination (to produce SERRS) is multiplicative. Thus, a log normal (or tailed) rather than a normal distribution of intensities across the slide is expected.[58] This is exactly what is shown in Fig. 8b. Most of the surface presents signal levels smaller than the average (there are also spots with no SERRS signal), but the SERRS from a few spots can be much larger than the average value.

Similar results were obtained with a 100× objective and are presented in Fig. 9. The higher magnification and NA of the

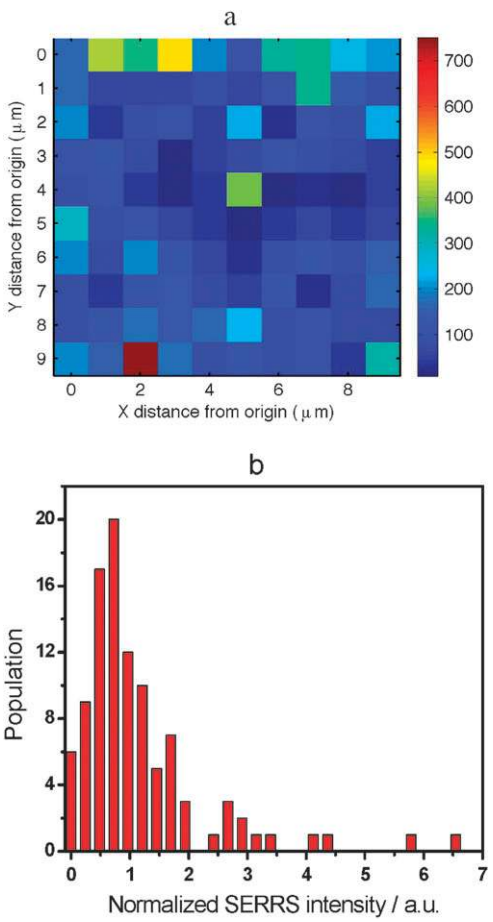

Fig. 8 (a) SERRS mapping of the 593 cm^{-1}-band of NBA; (b) histogram of the spatial distribution of SERRS intensity. 60 s accumulation. Concentration of NBA 2 ng/mL. 7 Ag NPs deposition. Laser excitation at 632.8 nm.

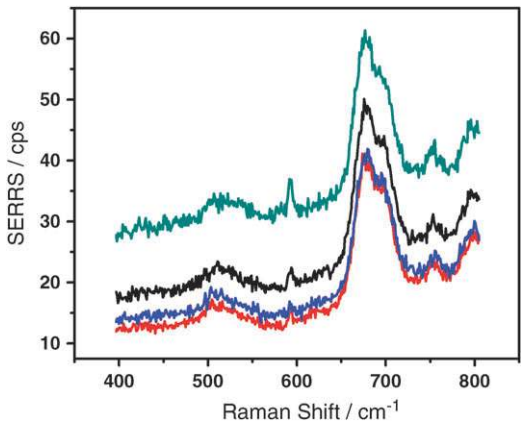

Fig. 9 SERRS spectra of NBA using a 100× objective from different spots at the same slide. Experimental conditions are the same as in Fig. 8. But only about 44 molecules are estimated in the laser spot. Laser excitation at 632.8 nm.

100× lens allow the illumination of an even smaller spot size, probing a smaller number of molecules. A weak NBA signal is still present under these conditions. Since only 44 molecules are estimated in the laser-illuminated area, and not all of them will be at hot spots, it is likely that these results are approaching the single-molecule limit. No blinking was observed in our case, indicating that the molecules are immobilized in the hot spot in the dry conditions of our experiments.

The performance of the substrate at near IR excitation was also probed. Fig. 10 shows the SERS from different concentrations of NBA obtained using 785 nm laser excitation. Since NBA has no electronic absorption in this region, the Raman enhancement does not benefit from a resonance Raman mechanism, as was the case for the 632.8 nm excitation. Thus, the relative SERS signal is not as strong as for the 632.8 nm excitation, and the interference of the background signal from the substrate is much more severe (Fig. 10 inset). In this case, the LOD determined using the same procedure as for 632.8 nm, was about 28 zeptomoles (2.8×10^{-20} moles) of

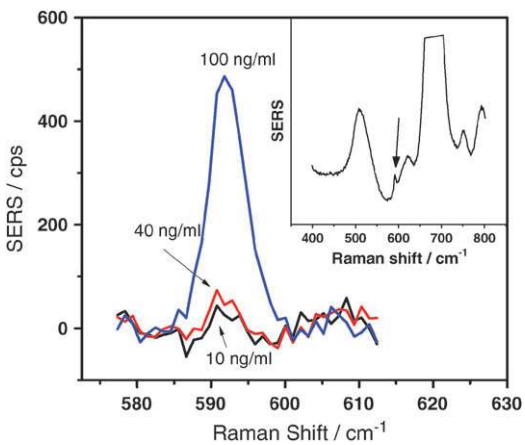

Fig. 10 SERS spectra of NBA at different concentrations (785 nm laser). Each spectrum is the average of 5 measurements at different spots on the same slide. Inset shows an extended spectrum for 100 ng/mL of NBA. The arrow indicates the NBA band. The other strong features are the background from the substrate.

molecules (10 ng/mL, 50× objective, numerical aperture (NA) = 0.75). Note that the laser spot at 785 nm is larger (see Experimental section for details).

IV. Conclusion

In this report, we used a multi-step deposition procedure to immobilize Ag NPs on glass using MPTMS sol–gel as linker. The procedure yielded highly sensitive SERS substrates. It is found that the Raman signal was dramatically enhanced (up to 3 orders of magnitude compared to just one deposition for both lasers (visible and near IR)) after 7 Ag NPs depositions. SERRS mapping showed that the number of hot spots increased with the deposition number, and the spatial distribution of intensities follows normal statistics when the surface is covered by a homogeneous distribution of nanofeatures. The spatial and sample to sample variability of the SE(R)RS intensities were less than 20% in this case. Detectable SERRS signal was observed even when the number of molecules in the laser spot was less than 100. Single molecule sensitivity is likely achieved, since not all molecules will populate the hottest spots. Even without the extra contribution from resonant Raman effects, the detection limit from these substrates is at the sub-zeptomolar level for the dyes tested.

Acknowledgements

This work was supported by operating grants from NSERC. The equipment grant was provided by the Canada Foundation for Innovation (CFI), the British Columbia Knowledge and Development Fund (BCKDF) and the University of Victoria through the New Opportunities Program.

References

1 A. G. Brolo, D. E. Irish and B. D. Smith, *J. Mol. Struct.*, 1997, **405**, 29–44.
2 A. Campion and P. Kambhampati, *Chem. Soc. Rev.*, 1998, **27**, 241–250.
3 M. Moskovits, *J. Raman Spectrosc.*, 2005, **36**, 485–496.
4 T. Vo-Dinh, *TrAC, Trends Anal. Chem.*, 1998, **17**, 557–582.
5 G. A. Baker and D. S. Moore, *Anal. Bioanal. Chem.*, 2005, **382**, 1751–1770.
6 B. D. Moore, L. Stevenson, A. Watt, S. Flitsch, N. J. Turner, C. Cassidy and D. Graham, *Nat. Biotechnol.*, 2004, **22**, 1133–1138.
7 C. M. Ruan, W. Wang and B. H. Gu, *Anal. Chem.*, 2006, **78**, 3379–3384.
8 J. Kneipp, H. Kneipp and K. Kneipp, *Chem. Soc. Rev.*, 2008, **37**, 1052–1060.
9 W. E. Doering, M. E. Piotti, M. J. Natan and R. G. Freeman, *Adv. Mater.*, 2007, **19**, 3100–3108.
10 X. M. Qian and S. M. Nie, *Chem. Soc. Rev.*, 2008, **37**, 912–920.
11 G. Braun, S. J. Lee, M. Dante, T. Q. Nguyen, M. Moskovits and N. Reich, *J. Am. Chem. Soc.*, 2007, **129**, 6378–6379.
12 L. G. Olson, Y. S. Lo, T. P. Beebe and J. M. Harris, *Anal. Chem.*, 2001, **73**, 4268–4276.
13 L. G. Olson, R. H. Uibel and J. M. Harris, *Appl. Spectrosc.*, 2004, **58**, 1394–1400.
14 M. Moskovits, in *Surface-Enhanced Raman Scattering: Physics and Applications*, 2006, vol. 103, pp. 1–17.
15 P. Etchegoin, L. F. Cohen, H. Hartigan, R. J. C. Brown, M. J. T. Milton and J. C. Gallop, *J. Chem. Phys.*, 2003, **119**, 5281–5289.
16 E. C. Le Ru, P. G. Etchegoin and M. Meyer, *J. Chem. Phys.*, 2006, **125**.

17 M. G. Albrecht and J. A. Creighton, *J. Am. Chem. Soc*., 1977, **99**, 5215–5217.
18 M. J. Natan, *Faraday Discuss*., 2006, **132**, 321–328.
19 J. Henzie, M. H. Lee and T. W. Odom, *Nat. Nanotechnol*., 2007, **2**, 549–554.
20 E. S. Kwak, J. Henzie, S. H. Chang, S. K. Gray, G. C. Schatz and T. W. Odom, *Nano Lett*., 2005, **5**, 1963–1967.
21 R. Gordon, A. G. Brolo, A. McKinnon, A. Rajora, B. Leathem and K. L. Kavanagh, *Phys. Rev. Lett*., 2004, **92**.
22 A. Lesuffleur, L. K. S. Kumar, A. G. Brolo, K. L. Kavanagh and R. Gordon, *J. Phys. Chem. C*, 2007, **111**, 2347–2350.
23 R. Gordon, D. Sinton, K. L. Kavanagh and A. G. Brolo, *Acc. Chem. Res*., 2008, **41**, 1049–1057.
24 J. R. Anema, A. G. Brolo, P. Marthandam and R. Gordon, *J. Phys. Chem. C*, 2008, **112**, 17051–17055.
25 Q. Min, M. J. L. Santos, E. M. Girotto, A. G. Brolo and R. Gordon, *J. Phys. Chem. C*, 2008, **112**, 15098–15101.
26 G. Laurent, N. Felidj, J. Grand, J. Aubard, G. Levi, A. Hohenau, F. R. Aussenegg and J. R. Krenn, *Phys. Rev. B*, 2006, **73**.
27 G. Laurent, N. Felidj, S. L. Truong, J. Aubard, G. Levi, J. R. Krenn, A. Hohenau, A. Leitner and F. R. Aussenegg, *Nano Lett*., 2005, **5**, 253–258.
28 D. R. Ward, N. K. Grady, C. S. Levin, N. J. Halas, Y. P. Wu, P. Nordlander and D. Natelson, *Nano Lett*., 2007, **7**, 1396–1400.
29 L. D. Qin, S. L. Zou, C. Xue, A. Atkinson, G. C. Schatz and C. A. Mirkin, *Proc. Natl. Acad. Sci. USA*, 2006, **103**, 13300–13303.
30 Y. Lu, G. L. Liu, J. Kim, Y. X. Mejia and L. P. Lee, *Nano Lett*., 2005, **5**, 119–124.
31 R. F. Aroca, R. A. Alvarez-Puebla, N. Pieczonka, S. Sanchez-Cortez and J. V. Garcia-Ramos, *Adv. Colloid Interface Sci*., 2005, **116**, 45–61.
32 R. G. Freeman, K. C. Grabar, K. J. Allison, R. M. Bright, J. A. Davis, A. P. Guthrie, M. B. Hommer, M. A. Jackson, P. C. Smith, D. G. Walter and M. J. Natan, *Science*, 1995, **267**, 1629–1632.
33 C. J. Addison and A. G. Brolo, *Langmuir*, 2006, **22**, 8696–8702.
34 M. K. Fan and A. G. Brolo, *ChemPhysChem*, 2008, **9**, 1899–1907.
35 M. D. Musick, C. D. Keating, L. A. Lyon, S. L. Botsko, D. J. Pena, W. D. Holliway, T. M. McEvoy, J. N. Richardson and M. J. Natan, *Chem. Mater*., 2000, **12**, 2869–2881.
36 J. B. Jackson and N. J. Halas, *Proc. Natl. Acad. Sci. USA*, 2004, **101**, 17930–17935.
37 C. Peng, Y. Song, G. Wei, W. Zhang, Z. Li and W. F. Dong, *J. Colloid Interface Sci*., 2008, **317**, 183–190.
38 R. F. Aroca, P. J. G. Goulet, D. S. dos Santos, R. A. Alvarez-Puebla and O. N. Oliveira, *Anal. Chem*., 2005, **77**, 378–382.
39 K. W. Kho, Z. X. Shen, H. C. Zeng, K. C. Soo and M. Olivo, *Anal. Chem*., 2005, **77**, 7462–7471.
40 S. Zhao, K. Zhang, J. An, Y. Y. Sun and C. Q. Sun, *Mater. Lett*., 2006, **60**, 1215–1218.
41 A. Tao, F. Kim, C. Hess, J. Goldberger, R. R. He, Y. G. Sun, Y. N. Xia and P. D. Yang, *Nano Lett*., 2003, **3**, 1229–1233.
42 G. Wei, L. Wang, L. L. Sun, Y. H. Song, Y. J. Sun, C. L. Guo, T. Yang and Z. A. Li, *J. Phys. Chem. C*, 2007, **111**, 1976–1982.
43 N. P. W. Pieczonka, P. J. G. Goulet and R. F. Aroca, *J. Am. Chem. Soc*., 2006, **128**, 12626–12627.
44 X. L. Li, W. Q. Xu, J. H. Zhang, H. Y. Jia, B. Yang, B. Zhao, B. F. Li and Y. Ozaki, *Langmuir*, 2004, **20**, 1298–1304.
45 P. J. G. Goulet, D. S. dos Santos, R. A. Alvarez-Puebla, O. N. Oliveira and R. F. Aroca, *Langmuir*, 2005, **21**, 5576–5581.
46 S. Tan, M. Erol, A. Attygalle, H. Du and S. Sukhishvili, *Langmuir*, 2007, **23**, 9836–9843.
47 Y. Han, S. Sukhishvili, H. Du, J. Cefaloni and B. Smolinsko, *J. Nanosci. Nanotechnol*., 2008, **8**, 5791–5800.
48 S. Tan, M. Erol, S. Sukhishvili and H. Du, *Langmuir*, 2008, **24**, 4765–4771.
49 P. Ahonen, T. Laaksonen, A. Nykanen, J. Ruokolainen and K. Kontturi, *J. Phys. Chem. B*, 2006, **110**, 12954–12958.
50 S. W. Joo, S. W. Han and K. Kim, *J. Phys. Chem. B*, 2000, **104**, 6218–6224.
51 B. K. Jena and C. R. Raj, *Anal. Chem*., 2006, **78**, 6332–6339.
52 G. Bauer, J. Hassmann, H. Walter, J. Haglmuller, C. Mayer and T. Schalkhammer, *Nanotechnology*, 2003, **14**, 1289–1311.
53 A. Bertoluzza, C. Fagnano, M. A. Morelli, V. Gottardi and M. Guglielmi, *J. Non-Cryst. Solids*, 1982, **48**, 117–128.
54 M. A. Mondragon, V. M. Castano, J. Garcia and C. A. Tellez, *Vib. Spectrosc*., 1995, **9**, 293–304.
55 F. Akbarian, B. S. Dunn and J. I. Zink, *J. Raman Spectrosc*., 1996, **27**, 775–783.
56 Z. H. Zhu, T. Zhu and Z. F. Liu, *Nanotechnology*, 2004, **15**, 357–364.
57 D. W. Scott, *Biometrika*, 1979, **66**, 605–610.
58 E. Limpert, W. A. Stahel and M. Abbt, *Bioscience*, 2001, **51**, 341–352.